Sediment structure and physicochemical changes following tidal inundation at a large open coast managed realignment site

Dale, J., Cundy, A. B., Spencer, K. L., Carr, S. J., Croudace, I. W., Burgess, H. M. & Nash, D. J.

may remain and you are advised to consult the published version if you wish to cite from it.

1 **Sediment structure and physicochemical changes following tidal inundation**

2 **at a large open coast managed realignment site**

3 Jonathan Dale[1,2*], Andrew B. Cundy[3], Kate L. Spencer[4], Simon J. Carr[4,5], Ian W. Croudace[3],

4 Heidi M. Burgess[1] and David J. Nash[1,6]

5 [1]Centre for Aquatic Environments, School of Environment and Technology, University of

6 Brighton, Brighton, BN2 4GJ, UK.

7 [2]School of Energy, Construction and Environment, Coventry University, Coventry CV1 5FB,

8 UK.

9 [3]School of Ocean and Earth Science, University of Southampton, National Oceanography

10 Centre (Southampton), Southampton, SO14 3ZH, UK.

11 [4]School of Geography, Queen Mary University of London, London, E1 4NS.

12 [5]Science, Natural Resources & Outdoor Studies, University of Cumbria, Rydal Road,

13 Ambleside, Cumbria LA22 9BB, U.K.

14 [6]School of Geography, Archaeology and Environmental Studies, University of the

15 Witwatersrand, Private Bag 3, Wits 2050, South Africa.

16

17 ***Corresponding Author:**

18 Jonathan Dale

19   School of Environment and Technology, University of Brighton, Cockcroft Building, Lewes

20   Road, Brighton, UK, BN2 4GJ. Email: J.J.Dale@brighton.ac.uk

21

23

24

28

1 Abstract

Managed realignment (MR) schemes are being implemented to compensate for the loss of intertidal saltmarsh habitats by breaching flood defences and inundating the formerly defended coastal hinterland. However, studies have shown that MR sites have lower biodiversity than anticipated, which has been linked with anoxia and poor drainage resulting from compaction and the collapse of sediment pore space caused by the site's former terrestrial land use. Despite this proposed link between biodiversity and soil structure, the evolution of the sediment sub-surface following site inundation has rarely been examined, particularly over the early stages of the terrestrial to marine or estuarine transition. This paper presents a novel combination of broad- and intensive-scale analysis of the sub-surface evolution of the Medmerry Managed Realignment Site (West Sussex, UK) in the three years following site inundation. Repeated broad-scale sediment physiochemical datasets are analysed to assess the early changes in the sediment subsurface and the preservation of the former terrestrial surface, comparing four locations of different former land uses. Additionally, for two of these locations, high-intensity 3D-computed X-ray microtomography and Itrax micro-X-ray fluorescence spectrometry analyses are presented. Results provide new data on differences in sediment properties and structure related to the former land use, indicating that increased agricultural activity leads to increased compaction and reduced porosity. The presence of anoxic conditions, indicative of poor hydrological connectivity between the terrestrial and post-inundation intertidal sediment facies, was only detected at one site. This site has experienced the highest rate of accretion over the terrestrial surface (*ca*. 7 cm over 36 months), suggesting that poor drainage is caused by the

52 interaction (or lack of) between sediment facies rather than the former land use. This has

53 significant implications for the design of future MR sites in terms of preparing sites, their

54 anticipated evolution, and the delivery of ecosystem services.

55

56

2   Introduction

Saltmarsh and mudflat environments provide a range of ecosystem services (Costanza et al., 1997) including detoxification, nursery habitat and flood defence through the attenuation of wave energy (e.g. Moller et al., 2014; Rupprecht et al., 2017). However, these habitats are threatened by sea level rise, causing erosion and coastal squeeze (e.g. Doody, 2004), and anthropogenic pressures including pollution and reclamation in response to urbanisation and population growth. This has resulted in the loss and degradation of coastal habitats worldwide. In recent years, there have been a number of schemes implemented to compensate for these losses, frequently driven by legislative requirements to improve habitats and biodiversity such as the EU Habitats Directive (European Parliament and the Council of the European Commission, 1992). These schemes use ecological engineering (or ecoengineering) approaches (Bergen et al., 2001) and aim to restore the structure and function of intertidal environments, either through habitat creation or by engineering physical processes to create the desired conditions to encourage habitat creation (Elliott et al., 2016). This paper focuses on managed realignment (MR), one of the most popular coastal ecoengineering techniques.

MR describes the practice of inundating areas of the coastal hinterland through de-embanking, removing or breaching the former flood defences, with new defences constructed inland. Yet, growing evidence suggests that saltmarshes within MR sites have lower biodiversity and abundance of key species than anticipated (e.g. Mazik et al., 2010; Mossman et al., 2012), which may have consequences for ecosystem functioning (Doherty

80   et al., 2011). These differences have been associated with abiotic factors such as nutrient

81   availability, salinity and redox conditions (Erfanzadeh et al., 2010; Mossman et al., 2012).

82   MR is often carried out in areas of former saltmarsh and mudflat habitat, which have been

83   previously reclaimed through the construction of embankments and then drained for

84   agriculture. As a consequence, the practice results in the restoration and re-creation of

85   historical intertidal habitats (as opposed to creating "new" habitats). Reclamation and

86   drainage leads to compaction, de-watering and mineralisation of organic matter, resulting in

87   irreversible changes to the sub-surface sediment structure (including the collapse of pore

88   space) (e.g. Crooks and Pye, 2000; Hazelden and Boorman, 2001; Spencer et al., 2017). This

89   has led to poor drainage in many MR sites following site inundation and reduced vertical

90   hydrological connectivity between the relict terrestrial horizon and the freshly deposited

91   intertidal sediment (e.g. Crooks and Pye, 2000; Hazelden and Boorman, 2001; Tempest et

92   al., 2015).

93

94   The flux of pore water through the sub-surface sediment is considered to be crucial for

95   controlling abiotic conditions, and therefore could exert a major influence on vegetation

96   colonisation in MR sites (Davy et al., 2011; e.g. Howe et al., 2010; Wilson et al., 2015).

97   However, there remains a shortage of data on the evolution of sub-surface sediment

98   geotechnical and geochemical properties following inundation at MR sites (Esteves, 2013).

99   This is especially true for investigations into the critical period immediately following site

100   inundation (i.e. in the early stages of the terrestrial to marine or estuarine transition) as it is

101   these surface conditions that will form the substrate for seedling germination, with

102   particular focus required into:

103   (a) the preservation of the relict terrestrial horizon, and its structural, physical and

104   chemical characteristics, post-inundation, and

105   (b) the development of the sub-surface geochemical profile in response to the former

106   terrestrial land use.

107

108   This study investigates the impact of different pre-managed realignment land use practices

109   on the early evolution of the sub-surface sediment structure and geochemical environment

110   at the Medmerry Managed Realignment Site (West Sussex, UK), during the first three years

111   of site inundation (covering the early stages of the transition from a terrestrial to a marine /

112   coastal lagoonal system). Specifically, a novel combination of broad- (centimetre to

113   decimetre) and intensive- (micron) scale sedimentary data sets, from samples taken at two

114   time points, are analysed to assess the differences and the early evolution of the sub-

115   surface geochemical profile and sediment structure for sites of differing former land use.

116   The implications of these differences for the longer term development of sediment

117   structure, drainage and physicochemical properties, in relation to site evolution,

118   management, and ecosystem service delivery, are discussed and assessed.

119

120   **3   Study Site**

121

122   The Medmerry Managed Realignment Site (Figure 1) is located within the Solent, southern

123   UK, on the western side of the Manhood Peninsula (Figure 1, insert). Previously, the area

124   had been a brackish lagoon (Krawiec, 2017) behind a shingle barrier beach, which had

125   drained through Pagham Harbour on the eastern side of the peninsula. However, this area

126   was separated from Pagham Harbour and reclaimed through the construction of an

127   embankment, and subsequently drained, between 1805 and 1809 (Bone, 1996). Coastal

128   flood defence for the reclaimed area at Medmerry was provided by the shingle barrier

129   beach, which was managed by the Environment Agency (UK). To maintain the necessary

130   defence standard, constant work was required each winter to recycle and re-profile the

131   shingle bank. Nevertheless, the defences remained vulnerable during storm events; the

132   bank was breached 14 times between 1994 and 2011, flooding homes, local holiday caravan

133   parks and agricultural land. The coastal flooding and erosion risk was reviewed in the

134   Pagham to East Head Coastal Defence Strategy (Environment Agency, 2007), which

135   endorsed MR as the most suitable method of managing the risk of coastal flooding.

136

137   The Medmerry scheme, which is the largest open coast MR site in Europe (at the time of site

138   inundation), was designed not only to provide a sustainable and cost-effective method of

139   coastal flood risk management, but also to compensate for saltmarsh and mudflat habitat

140   loss elsewhere in the region. Over 80% of the Solent's coastline is designated for its nature

141   conservation interest (Foster et al., 2014), yet 40% (approximately 670 hectares) of

142   saltmarsh in the region were lost through erosion between 1971 and 2001 (Cope et al.,

143   2008). Over the one hundred years following construction of the Medmerry site, it was

144   estimated that up to 184 hectares of new intertidal and transitional habitat would be

145   created (Pearce et al., 2011).

146

147   Construction of the site began in autumn 2011, which included 7 km of new earth "bund"

148   defences, reaching 3 km inland. Freshwater drains through the site via four drainage outlets

149   with tidal gates constructed into the new defences. The site was breached on 9th

150   September 2013 through a single narrow opening in the shingle bank, forming a semi-

151   diurnal, mesotidal, semi-enclosed, fetch and depth limited estuarine system. At the time of

152   this study, high water at the furthest point inland occurred approximately 50 minutes after

153   high water at the breach (Dale et al., 2018b). During low tide, draining water is constricted

154   to the main channels running through the site (Figure 1), which in some cases drain to near

155   emptiness. Sediment is imported, and exported, from the wider coastal environment, but

156   Dale et al. (2018b) identified that larger concentrations are currently being internally

157   redistributed as the site responds to the introduction of intertidal inundation.

158

4   Materials and Methods

Six sediment cores were taken from the Medmerry site in each of 2015 and 2016. All sampling was performed at low water. Cores 1 to 4 were collected for broad-scale analysis, Cores 5 and 6 for intensive-scale analysis. Sampling was carried out at four locations within the Medmerry site. These locations were selected based on differences in former (terrestrial) land use. Cores 1 and 5 were taken from a former area of pastoral land, occasionally used for low quality (usually unsuccessful) arable agriculture. Cores 2 and 3 were from a former area of pastoral land, with Core 2 taken from a non-vegetated surface and Core 3 from a vegetated surface. Cores 4 and 5 were from a former intensive arable field, last harvested two weeks prior to site inundation, behind an area of lower elevation land which has experienced rapid accretion of coarse grained sandy sediment (d_{50} = 47.33 ± 0.91 μm) following site inundation (Dale et al., 2017). The expected differences in sediment structure as a result of the former land use are outlined in Table 1. The presence and extent of these proposed differences were assessed initially on a broad centimetre scale, followed by analysis carried out on an intensive (micron) scale.

4.1   Sampling and Methods for Broad (centimetre to decimetre)-Scale Analysis

Vertical sediment cores were taken in January 2015, 16 months after the site was breached, and September 2016, 36 months after site inundation, to evaluate differences in the sediment sub-surface physical properties and geochemistry. Two cores were taken in

10

181   parallel, at approximately the same elevation (± 2 cm) and within 30 cm of each other, at

182   each sampling location using a hand driven large (5cm diameter, stainless steel) gouge

183   corer, transferred to open PVC tubes and wrapped in PVC film. Due to topographic

184   variations within the site it was not possible to sample at identical elevations at the four

185   sampling sites, but all sites were approximately in the same position in the intertidal zone

186   and therefore are expected to have similar hydroperiod conditions. Core depths varied

187   between 26 and 49 cm, although parallel cores were not always taken to the same depth.

188   Sediment cores were collected at least 15 m from the channel to minimise the influence of

189   lateral sub-surface flow (Marani et al., 2006).

190

191   Samples were stored at + 3.6 °C until analysis. Sediment properties were visually described

192   and one core from each site was subsampled at 1 cm depth increments. Following hydrogen

193   peroxide treatment and dispersion with sodium hexametaphosphate, a Malvern

194   Instruments Mastersizer Hydro 2000G Laser Diffraction Particle Size Analyser was used to

195   determine the grain size distribution in sediment subsamples. Subsamples were also

196   examined for a suite of elements using an Inductively Coupled Plasma-Optical Emission

197   Spectrometer (ICP-OES). Samples were digested with Aqua Regia (modified from Berrow

198   and Stein, 1983). Aqua Regia was prepared with a 30% HNO_3 : 70% HCL (1:3) mixture at

199   room temperature. 0.1 ± 0.01 g of sample, oven dried at 105 °C, was digested in 3 ml of

200   Aqua Regia for three hours in a water bath at 80 °C. Following digestion, 7 ml of distilled

201   water were then added to the sample. A 1:10 dilution of the solution was made with

202   distilled water for analysis using a Perkin Elmer Optima 2100 DV ICP-OES. To assess the

203   elemental recovery of the digestion procedure the measured values were compared to the

204   quoted values for a Certified Reference Material (CRM) digested and analysed alongside the

205   samples (e.g. Cochran et al., 1998). The Mess-4 Marine Sediment (National Research Council

206   Canada) CRM was used and recovery values were generally within ± 25% of the reported

207   values (see supporting information). Process blanks and repeat samples were analysed

208   every 20 samples for quality control and analytical error. Process blanks were below

209   detection limits and repeat samples were within ±10 % throughout.

210

211   For the remaining cores, a known quantity of sediment was extracted using a syringe at 1

212   cm intervals and analysed for wet bulk density, moisture content, porosity and loss on

213   ignition (a proxy for organic content). The moisture content was measured as a percentage

214   of the dry mass (moisture content = water weight / dry sediment weight x 100) after

215   samples had been oven dried at 105 °C for 48 hours. Porosity was calculated using the dry

216   bulk density, assuming a particle density of 2.65 g cm^{-3} as stated by (Rowell, 1994) based on

217   typical data. The organic content of the samples was estimated via the loss on ignition proxy

218   method, following ignition of subsamples for six hours at 450 °C.

219

220   **4.2   Sampling and Methods for Intensive (micron)-Scale Analysis**

221

222   Smaller sediment cores were recovered from the same coring locations as Core 1 and Core

223   4, labelled Cores 5 and 6 respectively, in July 2015 and September 2016. These sites were

224   selected to analyse the influence that different intensities of arable agricultural activity have

225   on the subsurface sediment structure (i.e. by using sites with / without a history of intensive

226   arable agriculture). Cores were taken from within 2 m of the broad-scale coring sites, using

227   the advanced trimming method (Hvorslev, 1949). 44 mm diameter clear PVC tubes were

228   inserted into the sediment, trimming the surrounding sediment to minimise the disturbance

229   to the sample. Core lengths varied between 7.9 cm and 11.1 cm. The ends of the sample

230   tubes were capped and wrapped in PVC film secured with tape to prevent moisture loss.

231   Cores were kept upright during transport and storage to minimise any disturbance and, on

232   return to the laboratory, were stored between + 3.6 °C and + 4 °C.

233

234   3D-computed X-ray microtomography (μCT) is a non-destructive imaging method that has

235   been successfully applied to the study of saltmarsh sediment structure (Cnudde and Boone,

236   2013; Ketcham and Carlson, 2001; Spencer et al., 2017). μCT analysis was carried out here to

237   identify the sediment bulk phases and stratigraphy (for an assessment of the comparability

238   of the broad- and intensive-scale methodologies) and to analyse the key structural and

239   stratigraphic differences (total porosity, characterisation of the pore networks) between the

240   two sampled sites, at a much higher resolution than the broad-scale approach described

241   above. Whilst only single core samples were analysed in both years per core site, previous

242   analysis of this type (e.g. Spencer et al., 2017) has recognised that single core samples may

243   be used as a representation of the sediment structural characteristics. Sealed core tubes

244   were scanned at 76 μm resolution using a Nikon Metrology XT H 225 X-ray CT system with

245   Perkin Elmer XRD 0820 CN3 16-bit flat panel detector at Queen Mary, University of London.

246   Inspect-X was used to perform the scans and X-radiogram acquisition and reconstruction

247   was undertaken in CTPro. Drishti 2.1 volume rendering software was used for visualisation

248   of the reconstructed 3D models to identify bulk phases and inform segmentation following

249   the method of Spencer et al. (2017). Each 3D volume was sub-sampled further into four

250   equally sized depth increments, labelled A (base) to D (top), for detailed quantification of

251   differences in porosity with depth.

252

253   Cores were split vertically, photographed and analysed using Itrax non-destructive micro-X-

254   ray fluorescence spectrometry analysis (Croudace et al., 2006) for a range of elemental data

255   to compare changes in geochemistry with sediment structure analysis provided by the μCT,

256   at a 200 micrometre scale which was not possible using ICP-OES analysis. The Itrax produces

257   elemental data in counts but previous studies (e.g. Miller et al., 2014) have shown that

258   these data correlate well with quantitative analytical data (e.g., ICP-OES or Wavelength

259   Dispersive X-ray Fluorescence). Furthermore, the high frequency compositional changes

260   identified using the Itrax are often missed when analysing lower resolution bulk sub-

261   samples using more traditional, destructive, analytical methods. Each core was loaded onto

262   a horizontal cradle and scanned at a resolution of 200 μm at the BOSCORF laboratories,

263   National Oceanography Centre (Southampton). Cores were scanned wet to preserve

264   internal structure, with the software correcting for water content. Core Scanner Navigator

265   software was used to control the scanner, and data were plotted and displayed using Q-

266   Spec software. The Itrax scanner combines an X-ray line camera with a narrow, parallel,

267   high-flux X-ray beam to record a radiograph at 55 kV. XRF analysis was performed at 30 kV

268   (using a Mo anode X-ray tube, counting time 30s). Data were plotted using ItraX-Plot,

269   described by Croudace et al. (2006).

270

5 Results

5.1 Broad-scale (centimetre to decimetre) Physicochemical Changes in the Subsurface (Cores 1 to 4, 2015 and 2016)

Sediment cores 1 to 4 exhibited clear vertical zonation and could be divided into three facies (from core base to core surface) based on the environmental and land use change known to have occurred at the Medmerry site; (i) a pre-reclamation intertidal unit (*Unit A*), (ii) a reclamation boundary and soil unit formed since site reclamation between 1810 and 1880 (*Unit B*), and (iii) a terrestrial boundary and post-breach intertidal unit dating from site inundation in September 2013 (*Unit C*). The depth, composition and structure of the three units varied between sites.

5.1.1 Physical Characteristics

Average physical sediment characteristics for the three units are presented in Table 2 (see supplementary material for core descriptions and full datasets). Wet bulk density ranged from 0.64 to 2.18 kg m^{-3} and tended to increase with depth. Both moisture content (36.62 – 123.08 %) and porosity (0.33 – 0.81) decreased with depth, whereas loss on ignition values varied from 3.24% to 19.21% and fluctuated through the sample. Coarser grained sediments were generally found in the Unit A, compared to Units B and C, except in Core 4 where coarser grained sediments (d_{50} = 67.87 (2015) and 49.77 (2016)) were found at the sediment

15

293   surface. Median grain sizes ranged from 5.46 to 46.48 μm, and the mud content (clay + silt)

294   varied between 54.1 and 97.67 %. Statistical differences between sediment units were

295   assessed via a Kruskal Wallis test (n = 22 to 45, p < 0.05) for the whole dataset with the

296   exception of Core 4_{16} as no vertical zonation was found in this sample. Statistical differences

297   were found between the three sediment units for all parameters except for particle size

298   analysis (median grain size and mud content).

299

300   **5.1.2   Geochemical Profiles**

301

302   ICP-OES-derived major element data (Al, Ca, Fe, Mn, S, Na) are presented for 2015 (Figure 2)

303   and 2016 samples (Figure 3). To account for variations in sediment composition, data have

304   been normalised to Al (after Spencer et al., 2008). Ca decreased with depth through Unit C

305   in all 2015 samples and Cores 2 and 3 in 2016. This may be the result of decalcification,

306   typical of oxic saltmarsh sediments as a result of a lowering of the pH caused by nitrification

307   and decomposition of organic matter (Luther and Church, 1988; Vranken et al., 1990), and

308   then re-precipitation at depth. However, the scale of the decrease, and subsequent increase

309   in Unit A (Core 1_{15} and Core 4_{15}) could also be indicative of the presence of finely

310   comminuted shell debris in the intertidal sediments (Units A and C).

311

312   The diagenetic cycles of Fe and Mn have been well documented for saltmarsh sediments

313   (e.g. Spencer et al., 2003; Zwolsman et al., 1993). A peak in Fe or Mn concentration may

314   indicate redox mobilisation and reprecipitation, whereas an increase in S may represent

16

315   bacterially-mediated reduction of sulphate and formation of early-diagenetic sulphide

316   minerals (Cundy and Croudace, 1995). In both years at coring locations 1, 2 and 4, and in

317   Core 3_{15}, Fe and Mn concentrations were relatively homogenous down core with some

318   variability within Unit B, potentially caused by residual Fe concretions from the legacy of

319   ploughing within this zone, without any consistent or clear peaks. This is suggestive of a

320   fluctuating water table through the sediment sub-surface, consistent with the visual

321   observations of Fe-stained mottled sediment in this zone (see supplementary material); this

322   may be the result of tidal variability causing changes in the redox boundary, preventing the

323   formation of a stable redox zone and a strong Fe and Mn peak (Cundy and Croudace, 1995;

324   Zwolsman et al., 1993). However, in Core 3_{16}, Fe fluctuated throughout the depths

325   examined, peaking in the middle terrestrial zone. A clearer trend was observed in the

326   concentration of Mn, which is more sensitive than Fe to changes in redox status, with Mn

327   peaking at the boundary between the post-breach intertidal and terrestrial facies suggesting

328   possible diagenetic enrichment of Mn. S concentration decreased with depth, matching the

329   changes in Na concentration, and therefore implying that variations in S are driven primarily

330   by the introduction and evaporation of sea water.

331

332   Principal component analysis (PCA) was performed on the entire dataset to differentiate

333   between the physical and geochemical characteristics of the different units. PCA is a data

334   reduction technique which calculates new variables, or principal components, from linear

335   combinations of the original parameters and has been used successfully elsewhere to

336   (partially) discriminate geochemical data in coastal sediments (e.g. Cundy et al., 2006). The

337   first principal component accounts for the greatest variability, with every subsequent

338   component accounting for less of the variability (Reid and Spencer, 2009). Therefore, PCA

339   allows for grouping of different depths based on their physicochemical variability. Results

340   reveal clear differences between the PCA scores for Units A and C (Figure 4). Unit B also

341   demonstrated some evidence of grouping, but overlapped the other two units.

342

343   **5.2   Intensive-scale (micron) Subsurface Structure Physicochemical Characteristics**

344

345   **5.2.1   Sediment Structure**

346

347   Representative µCT reconstructions of sediment structure, with a voxel size of 65 µm, are

348   presented for coring locations 5 (taken from an area of former lower intensity arable

349   agriculture) and 6 (an area of former high intensity arable agriculture) in Figure 5. Core 5

350   demonstrated a relatively consistent solid matrix phase (Figure 5a) in both years sampled,

351   with no separate sediment facies, suggesting there has been no (or very minimal) post-site

352   inundation deposition of sediment. This is despite the broad-scale geophysical analysis

353   suggesting that a small, 2 cm, new intertidal sediment unit was present. It is, therefore,

354   possible that these different units might be present, but that they are sufficiently similar in

355   sediment structure to be indistinguishable via µCT analysis. In contrast, structural

356   differences were clearly visible in Core 6_{15} (Figure 5b). Laminations were present in a

357   compact upper sediment facies, consisting of sandy sediment deposited following site

358   inundation, overlying the former terrestrial soil that had been used intensively for arable

359   agriculture up to two weeks prior to site inundation. A sharp, irregular boundary occurred

360   between the two units and is marked on Figure 5b. No evidence of the upper sediment

361   facies was found in the Core 6_{16} sample (Figure 5b), probably due to the local remobilisation

362   of sediment in response to observed changes in the site's hydrodynamics, and

363   morphological evolution in response to the introduction to intertidal inundation (Dale et al.,

364   2018a).

365

366   Macroporosity (pores > 80 µm; Beven and Germann, 2013) measurements and

367   characteristics are presented in Table 3, and plotted for each of the four sub-samples in

368   Figure 6. In Core 5_{15}, a large, interconnected, pore space was detected through the sample,

369   whereas the Core 5_{16} pore structure consisted of horizontal elongated macropore networks.

370   In Core 6_{15}, a sheet like macro-pore was detected across the division between the units,

371   although it is likely that this an artificial feature caused by the coring process (which

372   resulted in sediment cracking along this interface), with a large horizontal macropore

373   dominating the lower facies. There was also no evidence of this horizontal pore system in

374   Core 6_{16}, with the macropore network dominated by a vertical pore (on the left of the 2016

375   macro-pore phase in Figure 5b) and areas of isolated, flattened pore space.

376

377   Bulk macroporosity in Core 5 was generally moderate to high (5.6 – 22.4 %) and decreased

378   with depth (Figure 6), as would be expected due to sediment compaction effects. Less

379   variability was observed in Core 6, where bulk macroposity was low to moderate (3.5 – 13.1

380   %). The degree of pore connectivity is indicated by the Euler-Poincaré characteristic, a

381   measure of the number of redundant connections within the pore network expressed as a

382   function of the volume, with decreased connectivity indicated by increased positive values,

383   and increased connectivity demonstrated by decreased negative values (Vogel, 1997). All

384   samples followed a trend of decreasing connectivity upwards, and then increasing in the

385   upper sub-sample, reflecting an increase in redundant connections and more tortuous pore

386   networks in the upper and lower sediment sub-sections. Connectivity was greater in 2015

387   compared to 2016 at both sites and was greater in Core 5 compared to Core 6, suggesting

388   greater levels of compaction due to higher levels of agricultural activity and an increase in

389   compaction at both sites as each evolved following site inundation.

390

391   The mean number of branches per pore were calculated through the transformation of

392   macropores into topological networks of nodes and branches, and used as an indication of

393   pore network complexity (Polder et al., 2010). Pore networks were more complex in Core 6

394   than Core 5, but at both sites decreased in complexity between 2015 and 2016. This

395   suggests that pore system complexity decreases over time following site inundation, due to

396   either the hydraulic head of tidal water above the sediment causing compaction or

397   sediment being flushed out as the water drains causing the pore networks to collapse (Dale

398   et al., 2018a). No distinct pattern was present in the Core 5_{15}, but in Core 5_{16} the upper sub-

399   sample had a greater number of branches per pore compared to the rest of the sample. In

400   contrast, complexity in Core 6 decreased upwards, but increased in the upper sub-section

401   consisting of the post-breach sediment facies. The degree of anisotropy is representative of

402   similarity in arrangement and the directness of the branches of the dominant macropore

403   system (Odgaard, 1997). In 2015, pores were more aligned in Core 5 than Core 6, although

404   anisotropy was much lower in the basal sub-samples of Core 5 (A and B). Anisotropy was

405   higher in the post-breach sediment facies in Core 6_{15}. In comparison, macropores

406   demonstrated a similar level of organisation in Core 5_{16}, whereas Core 6_{16} had a higher

407   anisotropy value representing an increase in similarity in the arrangement of the pore

408   networks.

409

410   **5.2.2   Sediment Geochemistry**

411

412   Itrax scanning was employed to examine the variability of nine elements at high spatial

413   resolution (200 µm). The content of coarse grained sediment, indicated by the Zr and Cr

414   intensity (which are frequently associated with heavy mineral assemblages in detrital sands,

415   e.g. Cundy et al., 2006), remained relatively constant in Core 5_{15} (Figure 7a). Two major

416   peaks were observed in the Cr intensity, although the second of these peaks corresponded

417   with an area of high intensity present on the radiograph likely to be a clast. Measurements

418   of the K intensity indicate that the fine grained fraction decreased in the middle section of

419   the sample, increasing again deeper in the sample, which is also reflected in Si and the bulk

420   µCT attenuation measurements (Figure 5a). Similar trends were observed in the Cl and Ca

421   intensity. Black sediment, low Fe and Mn, and a peak in S, suggest possible bacterial

422   reduction of sulphate within the cracked and desiccated near-surface sediments (Figure 5a),

423   although broadly coincident peaks in Cl and Ca may indicate that the peak in S is at least

424   partly a function of increased porewater sulphate rather than sulphate reduction processes.

425   Fe and Mn increased below this unit and remained constant throughout the rest of the

426   sample, with three relatively large peaks. However, the Fe peaks corresponded with peaks

427   in X-ray intensity (kcps) and are likely to be the product of X-ray response rather than

428   increases in concentration. After peaking in the near-surface sediment, S followed a similar

429   pattern to Si, K, Cl and Ca.

430

431   No major vertical changes in bulk sediment composition were detected in Core 5_{16} (Figure

432   7b), demonstrated by the relatively constant distribution of Si with the major peaks

433   corresponding to variability in the X-ray response (kcps). These observations were

434   supported by similar trends in Zr and Cr intensities, although peaks were also observed in

435   these elements corresponding to the presence of high density material (clasts, evident in

436   the X-radiograph image). The distribution of K indicated relatively constant clay content

437   within the sample. Cl decreased slightly down-sample, whereas Ca decreased in the lower

438   section of the sample, indicative of decalcification. In contrast to the other elements, Mn

439   showed a strong increase in intensity in the middle part of the core, possibly reflecting early

440   diagenetic enrichment, although this observation was not supported by change in the Fe

441   intensity. However, analysis of the Fe / Mn ratio (Figure 8) indicated higher concentrations

442   of Mn to Fe in the middle of the core, suggesting mildly reducing conditions and early

443   diagenetic mobilisation of Mn. No evidence of the bacterial reduction of sulphate, possibly

444   present in the near-surface of the previous sample, was found, and trends in S generally

445   coincided with peaks in Cl and Ca so may be caused by increased porewater sulphate rather

446   than microbially-mediated sulphate reduction.

447

448   Coarse grained sediments dominated the near-surface component of Core 6_{16} (Figure 7c),

449   visible in the photographic image and indicated by the high intensity of Zr. Several peaks in

450   Cr were detected in the upper part of the core, likely to correspond to the laminations

451   observed in the μCT scan (Figure 5b). At the boundary between the post-breach and

452   terrestrial sediment facies Cr peaked below a unit of low density detected by the

453   radiograph, matching the sheet-like pore space present in the μCT scan (Figure 5b). Below

454   this unconformity, K intensity increased, and Zr / Cr decreased, indicating an increase in fine

455   grained sediment. Cl generally decreased through the sample, whereas Ca decreased and

456   then increased again. Evidence of sub-surface diagenetic enrichment of Mn was provided by

457   an increase, and peak, in intensity in the lower third of the core. The peak in Mn

458   corresponded to an area of low density measured by the radiograph, although this is not

459   visible on the photography. It is possible that this area is the large horizontal macro-pore

460   feature present in the μCT analysis. The concentration of Fe also increased through the

461   sample, with areas of enrichment corresponding to red mottling on the sample. The Fe / Mn

462   ratio decreased through the upper 2 cm of the sample (Figure 8), but increased again at a

463   similar depth to the large horizontal macro-pore. Below the terrestrial boundary, S intensity

464   decreased through the sample. Small scale increases in S intensity occurred in areas where

465   red mottling of the sediment was not present.

466

467   In Core 6_{16} (Figure 7d) coarser grained sediments were only found in the surface sediment,

468   indicated by the surface peak in Zr, consistent with the findings from the broad-scale and

469   μCT analysis. Trends in K suggested increased clay content was present in the middle of the

470   sample. A peak in Cl occurred within the upper sub-surface, corresponding to a peak in S,

471   which could indicate the depth of saline intrusion into the sediment. Fe and Mn decreased

472   through the top of the red mottled surface sediment. Fe, and to a lesser extent Mn,

473   increased through the middle of the sample, supporting visual observations of red mottling,

474   with an additional increase present in the deeper parts of the sample.

475

6   Discussion

6.1   Preservation of the Pre-Breach Terrestrial Surface

Observations made at other, older, MR sites suggest that visual changes in the sediment characteristics associated with a terrestrial boundary or horizon would no longer be present after a number of years. For example, no visual evidence of a terrestrial facies was found at Orplands Farm Managed Realignment Site 8 years after site inundation (Spencer et al., 2008), although at this site a terrestrial horizon could still be detected through analysis of physicochemical properties of the sediment. Broad-scale analysis from four locations at the Medmerry Managed Realignment Site provided visual evidence that a sub-surface unconformity could still be detected at all sites except for Core 4_{16}, the nearest site to the breach (in a significantly higher energy environment than the other sites sampled). However, no uniform stratigraphic marker of the terrestrial surface such as the organic rich peaty horizon identified at Pagham Harbour by Cundy et al. (2002) or the alternating peat-mud (i.e. terrestrial – marine) couplets used elsewhere as indicators of tectonic activity and sea level change in coastal and near-coastal sediments (e.g. Shennan et al., 1996; Shennan et al., 1998) was found, although these have been suggested to be inconsistently preserved in some suddenly submerged intertidal environments (Cundy et al., 2000). In each sample where a sub-surface unconformity was detected, a lower pre-reclamation sediment facies was also detected. PCA allowed (partial) discrimination of samples based on combined physical and geochemical sediment properties, as opposed to a single indicator such as loss

25

498   on ignition or changes in particle size, into groups which corresponded to one of the three

499   vertical sediment facies; post-breach, terrestrial or pre-reclamation sediments.

500

501   The reclamation of saltmarshes results in modification to sediment structure and properties

502   (e.g. Crooks et al., 2002; Hazelden and Boorman, 2001) as a result of de-watering and

503   organic matter mineralisation, decreasing the porosity and increasing the bulk density. After

504   the re-introduction of intertidal conditions through MR, the legacy of these changes can still

505   be detected, with low moisture contents still being found at depth several decades after site

506   inundation (Spencer et al., 2017). Analysis of sites of different former land use at Medmerry,

507   16 months after site inundation, indicated similar bulk densities and porosities within the

508   terrestrial facies regardless of former site activity and land use. However, moisture content

509   and loss on ignition were higher in Cores 2 and 3, areas which previously had not been

510   subjected to arable agricultural practices (i.e. ploughing).

511

512   Detailed examination of the 3D sediment structure through the use of µCT allowed

513   comparisons of the morphology and connectivity of the sediment macro-porosity at

514   different coring locations to be made. In Core 5, taken from a site that was previously used

515   occasionally (and usually unsuccessfully) for agriculture, no new intertidal sediment unit was

516   detected despite evidence of separate units in the broad-scale analysis. It is possible that

517   differences observed in the broad-scale analysis are the result of the terrestrial unit

518   transitioning into an intertidal sedimentary environment, rather than consisting of sediment

519   deposited following site inundation. This is reflected in the similarity in the matrix of the

520   sediment detected by the μCT analysis and the gradual transition between the units

521   observed in Core 1_{16}. Core 5 had a greater bulk macroporosity throughout the sediment

522   sub-surface, with simpler pore networks that were more connected and had greater

523   similarity in arrangement than Core 6, which had been used consistently for high intensity

524   agricultural activity. This indicates that, as a result of the legacy of different terrestrial

525   agriculture practices, different sub-surface structures exist in terms of sediment

526   macroporosity, which is likely to affect the drainage characteristics and therefore

527   geochemical profiles within the sediment subsurface. Terrestrial and post-breach facies

528   were detected in the 2015 3D sediment structural analysis performed on Core 6. The top

529   facies consisted of laminated sediment deposits, which had accreted post-site inundation.

530   When re-sampled, only one sediment facies was detected. This is potentially the result of

531   local remobilisation of intertidal sediment deposited post-site inundation, likely to be in

532   response to changes in site hydrodynamics and morphological evolution as the realignment

533   site evolves.

534

535   Analysis of physical characteristics and structure of the sediment at Medmerry indicate

536   differences in sediment composition, properties and macroporosity for sites of differing

537   former land use, with the terrestrial soil unit still detectable visibly at some sites up to three

538   years after site inundation. These differences may well have consequences for the

539   development of geochemical profiles, which might limit the colonisation of saltmarsh

540   vegetation (Davy et al., 2011) and explain the lower biodiversity and abundance of key

541   species observed elsewhere (e.g. Mazik et al., 2010; Mossman et al., 2012). Importantly,

542   however, levels of sediment accretion over the terrestrial unit were much lower than at

543   other older sites (typically 20 to 40 mm at Medmerry compared to, for example, *ca.* 60 mm

544   at Orplands Farm) (Spencer et al., 2008), which may partly mitigate any discontinuities in

545   hydrological connectivity caused by the deposition of intertidal sediment on top of the

546   preserved terrestrial surface.

547

548   **6.2   Implications for Geochemical Profile Development at Managed Realignment**

549   **sites**

550

551   Typical vertical saltmarsh geochemical profiles are controlled by strong physicochemical

552   gradients in pH and redox potential, and microbially-mediated organic matter breakdown

553   using electron acceptors such as O_2, MnO_2 and $Fe(OH)_3$ (e.g. Koretsky et al., 2005; Spencer

554   et al., 2003). Following reclamation and ploughing large-scale precipitation of Fe

555   oxyhydroxides and other Fe-rich minerals would be anticipated (Auxtero et al., 1991;

556   Violante et al., 2003). When re-introduced to intertidal conditions remobilisation of Fe by

557   the saline water is expected through dissimilatory reduction of sulphate or dissolved Fe

558   being re-distributed by advection caused by the local hydrology (Burton et al., 2011;

559   Johnston et al., 2011). However, impeded vertical solute and porewater transport caused by

560   the presence of an aquaclude-like boundary in the sediment sub-surface (e.g. Tempest et

561   al., 2015) may result in inadequate drainage, stagnant porewater and a lack of aeration. The

562   occurrence of these conditions will inevitably prevent the formation of suitable oxic

563   conditions for re-precipitation of Fe, and Mn, at the sediment surface (Spencer et al., 2008).

564

565   No evidence of an aquaclude was found in either of Cores 2 and 3. In Core 2_{15}, Fe peaked at

566   the terrestrial boundary, corresponding to a peak in loss on ignition values. The increase in

567   residual bulk organic matter, present on the terrestrial surface before site inundation, may

568   well drive bacterially-mediated sulphate reduction following incorporation into the

569   sediment, resulting in the enrichment of Fe via Fe-sulphide formation. No major trends

570   were detected in Fe content through the rest of the sample, where the sediment showed

571   clear red mottling, implying variability in the water table caused by tidal inundation (Cundy

572   and Croudace, 1995). Fe fluctuated through the red mottled Core 3_{15}, indicating a

573   fluctuating water column through the sub-surface sediment.

574

575   Core 2_{16} was visibly darker in the intertidal and terrestrial facies, decreasing in S and

576   increasing in Fe and Mn to the boundary between the units. The sharp nature of this

577   boundary, and the peak in moisture content may indicate reduced vertical conveyance of

578   water through the unconformity. The fluctuations in Fe, and to a lesser extent Mn, in the

579   pre-reclamation intertidal facies could be caused by trapping authigenic carbonate /

580   sulphide formation (Cundy and Croudace, 1995). In Core 3_{16}, the distribution of Fe

581   continued to indicate a fluctuating water column.

582

583   Broad- and intensive-scale analysis suggests evidence of bacterial reduction of sulphate at

584   the surface of Core 1_{15} and Core 5_{15}. Below this unit the red mottled sediment and Fe profile

585   implied a variable water column facilitated by the extensive inter-connected macro-pore

586   network indicated by μCT analysis. An increase in the Fe / Mn ratio in the middle of the

587   sample analysed using high resolution Itrax scanning in Core 5_{16} suggests redox mobilisation

588   of Mn, which is generally more sensitive to redox changes than Fe. Despite the differences

589   in sediment structure between Core 5 and 6, there was still evidence of Fe enrichment. The

590   macro-pore network was dominated by a large horizontal pore which corresponded to an

591   increase in the intensity of Mn and the Fe / Mn ratio in Itrax data, possibly the result of

592   enrichment via lateral through-flow and indicative that the pore was not an artificial by-

593   product of the sampling procedure. These trends were maintained when re-sampled with

594   no sub-surface unconformity detected in Core 6_{16}. Results presented here differ from the

595   geochemical and redox profiles observed in older MR sites (Spencer et al., 2008), and

596   natural saltmarsh and mudflat environments within the Solent (e.g. Cundy and Croudace,

597   1995). It remains to be seen if the geochemical profiles evolve in a similar manner to other

598   MR sites or towards that of a more typical intertidal setting, compared schematically in the

599   Graphical Abstract, and the timescales required for this development. Not only would this

600   determine the depth of any anoxic layer, which may inhibit biological activity, but will

601   influence nutrient exchange and the partitioning (and possibly release) of contaminants

602   such as metals or pesticides potentially stored within the sediment.

603

604   **6.3   Influence of the Former Land Use and Site Construction**

605

606   MR aims to restore the structure and functioning of intertidal habitats, compensating for

607   losses elsewhere. However, previous studies have demonstrated differences in the physical,

608   geochemical and hydrological characteristics of saltmarshes in MR sites, particularly at the

609   Orplands Farm site (UK), compared to natural marshes (Spencer et al., 2017; Spencer et al.,

610   2008; Tempest et al., 2015). This has resulted in the restoration of intertidal conditions, but

611   not full restoration of the hydrological regime and the physical structure of the intertidal

612   environment which may have consequences for the ecological functioning and ecosystem

613   services provided. It has been proposed that the structural differences between MR and

614   natural sites are the cause of water-logging and poor drainage, which have been attributed

615   to poor saltmarsh species abundance and diversity within MR sites (e.g. Mossman et al.,

616   2012). Clear differences in sediment structure for sites of different former land use were

617   found at the Medmerry Managed Realignment Site. Therefore, it would be anticipated that

618   sites with reduced porosity and pore connectivity would have lower subsurface flow, no or

619   low concentrations of dissolved oxygen, and anoxic sediment. However, analyses of the

620   geochemical profiles at Medmerry do not yet match this expectation.

621

622   Medmerry is still a developing site on the open coast and, therefore, has not experienced a

623   large accretion of intertidal sediment on the former terrestrial land surface, such as

624   observed in older MR sites found in sediment-rich estuarine environments (Spencer et al.,

625   2017; Spencer et al., 2008; Watts et al., 2003; Wolanski and Elliott, 2016). It remains to be

626   seen how the geochemical profiles develop following further accretion of sediment.

627   However, without the accretion of sediment on top of the terrestrial horizon, tidal waters

628   appear to have been able to drain through the terrestrial facies. An exception is the site of

629   Core 2; in the second sample taken from this site sediment appeared black and anoxic, with

630   evidence of water pooling at the terrestrial boundary and reduced hydrological connectivity

631   through the contact between the facies. These findings suggest that hydrological and

632   geochemical differences found in MR sites compared to natural saltmarshes are not caused

31

633   by sub-surface differences owing to the former land use, but by the formation of an

634   unconformity in the sediment column as a result of (a) the accretion of sediment, and (b)

635   sharp physicochemical contrasts between the accreted upper unit and the underlying

636   sediment. For the latter, in Core 2, it is likely that the formation of an anoxic unit has been

637   driven by the decay of terrestrial vegetation trapped and buried under the accreted

638   sediment following site inundation (French, 2006).

639

7   Conclusion

640

641

642   In this paper, differences in the sub-surface structure and physiochemical properties of

643   inundated sites with different former land use histories have been investigated at the

644   Medmerry Managed Realignment Site, during the initial 16 and 36 months after site

645   inundation. A novel combination of repeated broad- and intensive-scale analysis was used

646   to assess differences in the subsurface sediment structure and early geochemical evolution

647   in the three years following site inundation. Results indicate a number of new findings,

648   including:

649   • Clear differences are present in the sediment structure and properties at different

650   sites as a result of contrasts in the former land use. Broad-scale analysis suggests

651   sites formerly used more intensively for agricultural purposes have lower moisture

652   content and loss on ignition, with intensive-scale analysis suggesting pore networks

653   were more complex but were less connected and aligned at these sites.

654   • Evidence of reduced drainage and anoxic conditions, identified in previous studies

655   (e.g. Spencer et al., 2017; Tempest et al., 2015) as a result of modifications caused by

656   a site's terrestrial history, were not found at Medmerry except at the site which had

657   experienced the highest level of accretion (*ca*. 7 cm in 36 months).

658

659   Further work is now required to assess if the differences in sediment structure, identified in

660   this study, can be detected in other (including older) MR sites where greater levels of post-

661   site inundation accumulation have occurred. The findings in this study indicate that the

662   formation of an aquaclude, reducing vertical solute transfer between facies, is not a direct

663   consequence of changes to the sediment caused by the former land use, but is the result of

664   the accretion of sediment, coupled with sharp physicochemical contrasts between the

665   accreted upper layer and the underlying sediment. Many MR sites are designed to

666   accumulate sediment, but these findings highlight the need for improved awareness of

667   sediment accretion in decision-making in the design of MR sites, alongside hydrodynamic

668   and topographic considerations. While further work on other MR sites is needed to assess

669   how widespread this accretionary effect is, the data presented here indicate that sites need

670   to be designed to encourage rapid accumulation of intertidal sediment, burying the

671   terrestrial boundary and so minimising the effect of an aquaclude. Alternatively, predictions

672   need to be adjusted to anticipate reduced saltmarsh diversity abundance, and therefore

673   ecosystem services delivery, until sufficient sediment has been accreted.

674

675

676 **Acknowledgements**

677

687

688

References

690 Auxtero E, Shamshuddin J, Paramananthan S. Mineralogy, morphology and classification of
691   acid sulfate soils in Pulau Lumut, Selangor. Pertanika 1991; 14: 43-51.

692 Bergen SD, Bolton SM, L. Fridley J. Design principles for ecological engineering. Ecological
693   Engineering 2001; 18: 201-210.

694 Berrow ML, Stein WM. Extraction of metals from soils and sewage sludges by refluxing with
695   aqua regia. Analyst 1983; 108: 277-285.

696 Beven K, Germann P. Macropores and water flow in soils revisited. Water Resources
697   Research 2013; 49: 3071-3092.

698 Bone AE. The shaping of the Selsey coastline: a review of the geomorphology, archaeology
699   and history. Tertiary Research 1996; 16: 5-14.

700 Burton ED, Bush RT, Johnston SG, Sullivan LA, Keene AF. Sulfur biogeochemical cycling and
701   novel Fe-S mineralization pathways in a tidally re-flooded wetland. Geochimica Et
702   Cosmochimica Acta 2011; 75: 3434-3451.

703 Cnudde V, Boone MN. High-resolution X-ray computed tomography in geosciences: A review
704   of the current technology and applications. Earth-Science Reviews 2013; 123: 1-17.

705 Cochran JK, Hirschberg DJ, Wang J, Dere C. Atmospheric deposition of metals to coastal
706   waters (Long Island Sound, New York USA): Evidence from saltmarsh deposits.
707   Estuarine Coastal and Shelf Science 1998; 46: 503-522.

708 Cope S, Bradbury A, Gorczynska M. Solent Dynamic Coast Project: Main Report; A tool for
709   SMP2, New Forest District Council/Channel Coastal Observatory, 2008.

710 Costanza R, d'Arge R, deGroot R, Farber S, Grasso M, Hannon B, et al. The value of the
711   world's ecosystem services and natural capital. Nature 1997; 387: 253-260.

712 Crooks S, Pye K. Sedimentological controls on the erosion and morphology of saltmarshes:
713   implications for flood defence and habitat recreation. In: Pye K, Allen JRL, editors.
714   Coastal and Estuarine Environments: Sedimentology, Geomorphology and
715   Geoarchaeology. 175, 2000, pp. 207-222.

716 Crooks S, Schutten J, Sheern GD, Pye K, Davy AJ. Drainage and elevation as factors in the
717   restoration of salt marsh in Britain. Restoration Ecology 2002; 10: 591-602.

718 Croudace IW, Rindby A, Rothwell RG. ITRAX: description and evaluation of a new multi-
719   function X-ray core scanner. Geological Society, London, Special Publications 2006;
720   267: 51-63.

721 Cundy AB, Croudace IW. Sedimentary and geochemical variations in a salt-marsh mud flat
722   environment from the mesotidal Hamble estuary, southern England. Marine
723   Chemistry 1995; 51: 115-132.

724 Cundy AB, Kortekaas S, Dewez T, Stewart IS, Collins PEF, Croudace IW, et al. Coastal
725   wetlands as recorders of earthquake subsidence in the Aegean: a case study of the
726   1894 Gulf of Atalanti earthquakes, central Greece. Marine Geology 2000; 170: 3-26.

727 Cundy AB, Long AJ, Hill CT, Spencer C, Croudace IW. Sedimentary response of Pagham
728   Harbour, southern England to barrier breaching in AD 1910. Geomorphology 2002;
729   46: 163-176.

730 Cundy AB, Sprague D, Hopkinson L, Maroukian H, Gaki-Papanastassiou K, Papanastassiou D,
731   et al. Geochemical and stratigraphic indicators of late Holocene coastal evolution in
732   the Gythio area, southern Peloponnese, Greece. Marine Geology 2006; 230: 161-
733   177.

734   Dale J, Burgess HM, Burnside NG, Kilkie P, Nash DJ, Cundy AB. The evolution of embryonic
735   creek systems in a recently inundated large open coast managed realignment site.
736   Anthropocene Coasts 2018a; 1: 16-33.
737   Dale J, Burgess HM, Cundy AB. Sedimentation rhythms and hydrodynamics in two
738   engineered environments in an open coast managed realignment site. Marine
739   Geology 2017; 383: 120-131.
740   Dale J, Burgess HM, Nash DJ, Cundy AB. Hydrodynamics and sedimentary processes in the
741   main drainage channel of a large open coast managed realignment site. Estuarine,
742   Coastal and Shelf Science 2018b.
743   Davy AJ, Brown MJH, Mossman HL, Grant A. Colonization of a newly developing salt marsh:
744   disentangling independent effects of elevation and redox potential on halophytes.
745   Journal of Ecology 2011; 99: 1350-1357.
746   Doherty JM, Callaway JC, Zedler JB. Diversity-function relationships changed in a long-term
747   restoration experiment. Ecological Applications 2011; 21: 2143-2155.
748   Doody JP. 'Coastal squeeze' - an historical perspective. Journal of Coastal Conservation
749   2004; 10: 129-138.
750   Elliott M, Mander L, Mazik K, Simenstad C, Valesini F, Whitfield A, et al. Ecoengineering with
751   Ecohydrology: Successes and failures in estuarine restoration. Estuarine, Coastal and
752   Shelf Science 2016; 176: 12-35.
753   Environment Agency. Pagham to East Head Coastal Defence Strategy, Worthing, 2007.
754   Erfanzadeh R, Garbutt A, Petillon J, Maelfait JP, Hoffmann M. Factors affecting the success
755   of early salt-marsh colonizers: seed availability rather than site suitability and
756   dispersal traits. Plant Ecology 2010; 206: 335-347.
757   Esteves LS. Is managed realignment a sustainable long-term coastal management approach?
758   Journal of Coastal Research 2013; Special Issue 65: 933-938.
759   European Parliament and the Council of the European Commission. Council directive
760   92/43/EEC of 21 May 1992 on the conservation of natural habitats and of wild fauna
761   and flora. Official Journal of the European Communities 1992; Series L206:
762   22.12.2000.
763   Foster NM, Hudson MD, Bray S, Nicholls RJ. Research, policy and practice for the
764   conservation and sustainable use of intertidal mudflats and saltmarshes in the Solent
765   from 1800 to 2016. Environmental Science & Policy 2014; 38: 59-71.
766   French PW. Managed realignment - The developing story of a comparatively new approach
767   to soft engineering. Estuarine Coastal and Shelf Science 2006; 67: 409-423.
768   Hazelden J, Boorman LA. Soils and 'managed retreat' in South East England. Soil Use and
769   Management 2001; 17: 150-154.
770   Howe AJ, Rodriguez JF, Spencer J, MacFarlane GR, Saintilan N. Response of estuarine
771   wetlands to reinstatement of tidal flows. Marine and Freshwater Research 2010; 61:
772   702-713.
773   Hvorslev MJ. Subsurface exploration and sampling of soils for civil engineering purposes.
774   Vicksburg, Mississippi: Waterways Experiment Station, 1949.
775   Johnston SG, Keene AF, Bush RT, Burton ED, Sullivan LA, Isaacson L, et al. Iron geochemical
776   zonation in a tidally inundated acid sulfate soil wetland. Chemical Geology 2011;
777   280: 257-270.
778   Ketcham RA, Carlson WD. Acquisition, optimization and interpretation of X-ray computed
779   tomographic imagery: applications to the geosciences. Computers & Geosciences
780   2001; 27: 381-400.

781   Koretsky CM, Van Cappellen P, DiChristina TJ, Kostka JE, Lowe KL, Moore CM, et al. Salt
782   marsh pore water geochemistry does not correlate with microbial community
783   structure. Estuarine, Coastal and Shelf Science 2005; 62: 233-251.
784   Krawiec K. Medmerry, West Sussex, UK: Coastal Evolution from the Neolithic to the
785   Medieval Period and Community Resilience to Environmental Change. The Historic
786   Environment: Policy & Practice 2017; 8: 101-112.
787   Luther GW, Church TM. Seasonal cycling of sulfur and iron in porewaters of a Delaware salt-
788   marsh. Marine Chemistry 1988; 23: 295-309.
789   Marani M, Silvestri S, Belluco E, Ursino N, Comerlati A, Tosatto O, et al. Spatial organization
790   and ecohydrological interactions in oxygen-limited vegetation ecosystems. Water
791   Resources Research 2006; 42.
792   Mazik K, Musk W, Dawes O, Solyanko K, Brown S, Mander L, et al. Managed realignment as
793   compensation for the loss of intertidal mudflat: A short term solution to a long term
794   problem? Estuarine, Coastal and Shelf Science 2010; 90: 11-20.
795   Miller H, Croudace IW, Bull JM, Cotterill CJ, Dix JK, Taylor RN. A 500 Year Sediment Lake
796   Record of Anthropogenic and Natural Inputs to Windermere (English Lake District)
797   Using Double-Spike Lead Isotopes, Radiochronology, and Sediment Microanalysis.
798   Environmental Science & Technology 2014; 48: 7254-7263.
799   Moller I, Kudella M, Rupprecht F, Spencer T, Paul M, van Wesenbeeck BK, et al. Wave
800   attenuation over coastal salt marshes under storm surge conditions. Nature
801   Geoscience 2014; 7: 727-731.
802   Mossman HL, Brown MJH, Davy AJ, Grant A. Constraints on Salt Marsh Development
803   Following Managed Coastal Realignment: Dispersal Limitation or Environmental
804   Tolerance? Restoration Ecology 2012; 20: 65-75.
805   Odgaard A. Three-dimensional methods for quantification of cancellous bone architecture.
806   Bone 1997; 20: 315-328.
807   Pearce J, Khan S, Lewis P. Medmerry managed realignment–sustainable coastal
808   management to gain multiple benefits. ICE Coastal Management. Innovative Coastal
809   Zone Management: Sustainable Engineering for a Dynamic Coast., Belfast, UK, 2011.
810   Polder G, Hovens H, Zweers A. Measuring shoot length of submerged aquatic plants using
811   graph analysis. Proceedings of the ImageJ User and Developer Conference 2010,
812   Mondorf-les-Bains, Luxembourg, 27-29 October 2010, 2010, pp. 172-177.
813   Reid MK, Spencer KL. Use of principal components analysis (PCA) on estuarine sediment
814   datasets: The effect of data pre-treatment. Environmental Pollution 2009; 157:
815   2275-2281.
816   Rowell DL. Soil science: Methods & applications. Harlow, Essex: Longman Scientific &
817   Technical, 1994.
818   Rupprecht F, Moller I, Paul M, Kudella M, Spencer T, van Wesenbeeck BK, et al. Vegetation-
819   wave interactions in salt marshes under storm surge conditions. Ecological
820   Engineering 2017; 100: 301-315.
821   Shennan I, Long AJ, Rutherford MM, Green FM, Innes JB, Lloyd JM, et al. Tidal marsh
822   stratigraphy, sea-level change and large earthquakes, i: a 5000 year record in
823   washington, U.S.A. Quaternary Science Reviews 1996; 15: 1023-1059.
824   Shennan I, Long AJ, Rutherford MM, Innes JB, Green FM, Walker KJ. Tidal marsh
825   stratigraphy, sea-level change and large earthquakes—ii: Submergence events
826   during the last 3500 years at Netarts Bay, Oregon, USA. Quaternary Science Reviews
827   1998; 17: 365-393.

828 Spencer KL, Carr SJ, Diggens LM, Tempest JA, Morris MA, Harvey GL. The impact of pre-
829   restoration land-use and disturbance on sediment structure, hydrology and the
830   sediment geochemical environment in restored saltmarshes. Science of The Total
831   Environment 2017; 587–588: 47-58.
832 Spencer KL, Cundy AB, Croudace IW. Heavy metal distribution and early-diagenesis in salt
833   marsh sediments from the Medway Estuary, Kent, UK. Estuarine Coastal and Shelf
834   Science 2003; 57: 43-54.
835 Spencer KL, Cundy AB, Davies-Hearn S, Hughes R, Turner S, MacLeod CL. Physicochemical
836   changes in sediments at Orplands Farm, Essex, UK following 8 years of managed
837   realignment. Estuarine Coastal and Shelf Science 2008; 76: 608-619.
838 Tempest JA, Harvey GL, Spencer KL. Modified sediments and subsurface hydrology in natural
839   and recreated salt marshes and implications for delivery of ecosystem services.
840   Hydrological Processes 2015; 29: 2346-2357.
841 Violante A, Barberis E, Pigna M, Boero V. Factors affecting the formation, nature, and
842   properties of iron precipitation products at the soil-root interface. Journal of Plant
843   Nutrition 2003; 26: 1889-1908.
844 Vogel HJ. Morphological determination of pore connectivity as a function of pore size using
845   serial sections. European Journal of Soil Science 1997; 48: 365-377.
846 Vranken M, Oenema O, Mulder J. Effects of tide range alterations on salt-marsh sediments
847   in the eastern Scheldt, SW Netherlands. Hydrobiologia 1990; 195: 13-20.
848 Watts CW, Tolhurst TJ, Black KS, Whitmore AP. In situ measurements of erosion shear stress
849   and geotechnical shear strength of the intertidal sediments of the experimental
850   managed realignment scheme at Tollesbury, Essex, UK. Estuarine Coastal and Shelf
851   Science 2003; 58: 611-620.
852 Wilson AM, Evans T, Moore W, Schutte CA, Joye SB, Hughes AH, et al. Groundwater controls
853   ecological zonation of salt marsh macrophytes. Ecology 2015; 96: 840-849.
854 Wolanski E, Elliott M. Estuarine Ecohydrology (Second Edition). Boston: Elsevier, 2016.
855 Zwolsman JJG, Berger GW, Vaneck GTM. Sediment accumulation rates, historical input,
856   postdepositional mobility and retention of major elements and trace-metals in salt-
857   marsh sediments of the Scheldt estuary, SW Netherlands. Marine Chemistry 1993;
858   44: 73-94.

859

860

861

Medmerry Managed Realignment Site (West Sussex, United Kingdom)		Orplands Farm Managed Realignment Site (Essex, United Kingdom)	Natural Saltmarsh (Hamble estuary, Hampshire, United Kingdom)
Post-site inundation intertidal	Physical properties varied in terrestrial unit but mottled oxic conditions were found throughout suggesting a variable water table and that vertical solute transfer is not inhibited	Post-site inundation: Poorly consolidated oxic unit with a high abundant root material and omplex, interconnected pore networks	Layer 1: Thin (mm) oxidised surface layer rich in plant litter
Terrestrial		Terrestrial: Firmer sediment layer, lower in organic and moisture content. Geochemical (lower Fe and Mn concentrations), structural (reduced pore distribution and complexity) and hydrological (reduced vertical water flux) evidences suggests reduced solute transfer between units	Layer 2: Mottled oxic zone with evidence of a fluctuating water table, rich in abundant (living) root material
Pre-reclamation intertidal			Layer 3: Black unit with reducing anoxic conditions, increased water content

Graphical Abstract: Schematic comparison of the sub-surface physicochemical properties of the sediment found at the Medmerry Managed Realignment Site (this study), Orplands Farm Managed Realignment Site, U.K. (Spencer et al., 2008; Tempest et al., 2015; Spencer et al., 2017) and a typical natural minerogenic saltmarsh (Cundy and Croudace, 1995). Not drawn to uniform vertical scale.
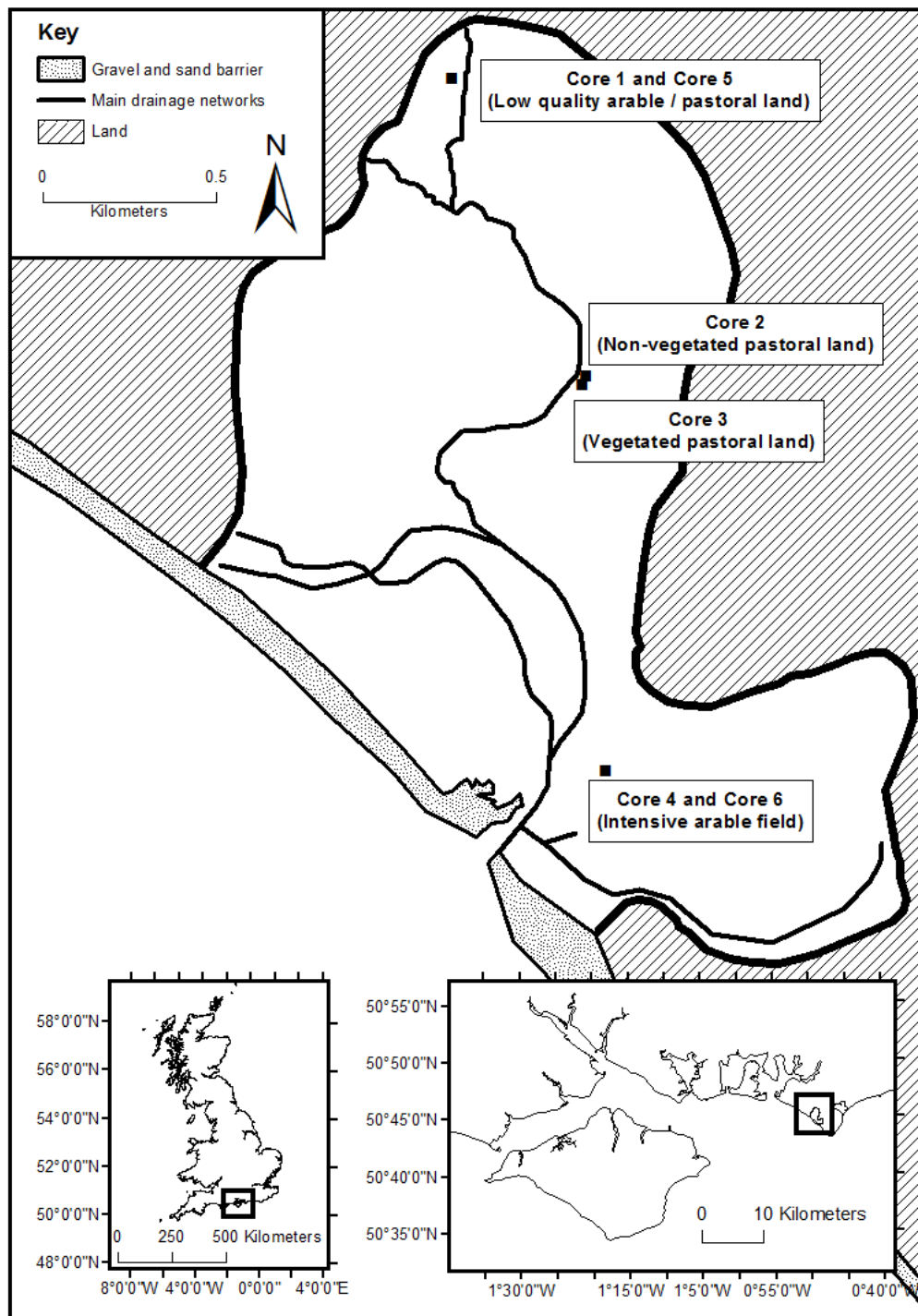
Figures

Figure 1: The Medmerry Managed Realignment Site (West Sussex, UK) and wider national (insert, left) and regional (insert, right) location. Coring locations are named and marked with black squares.
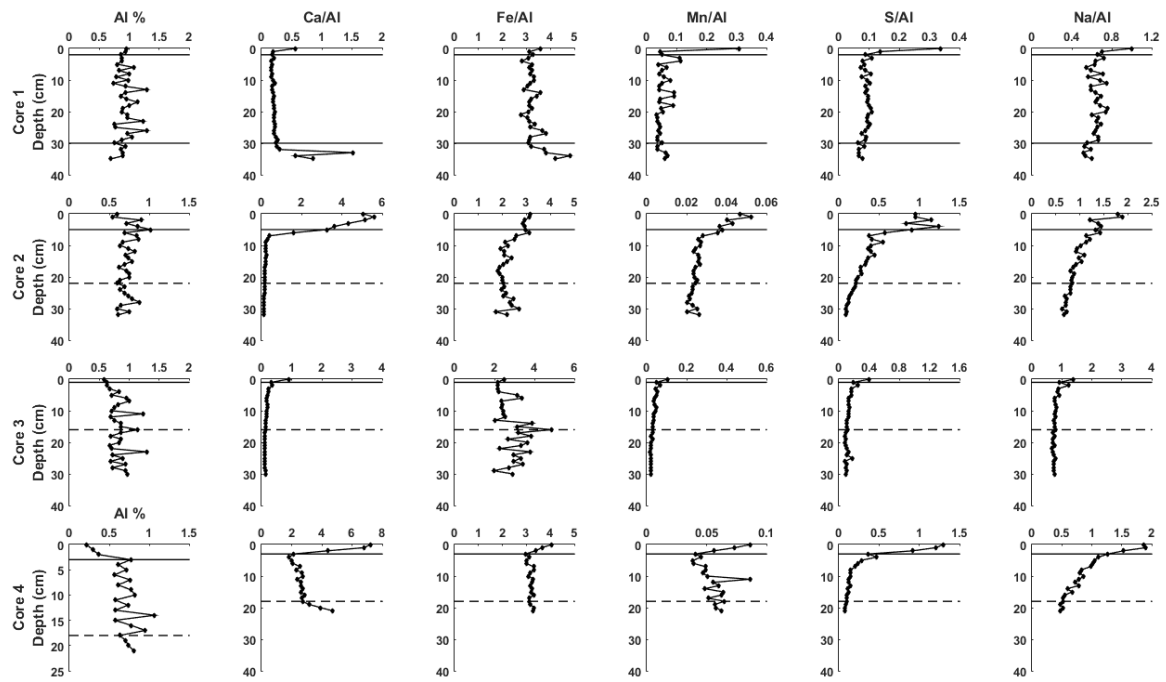
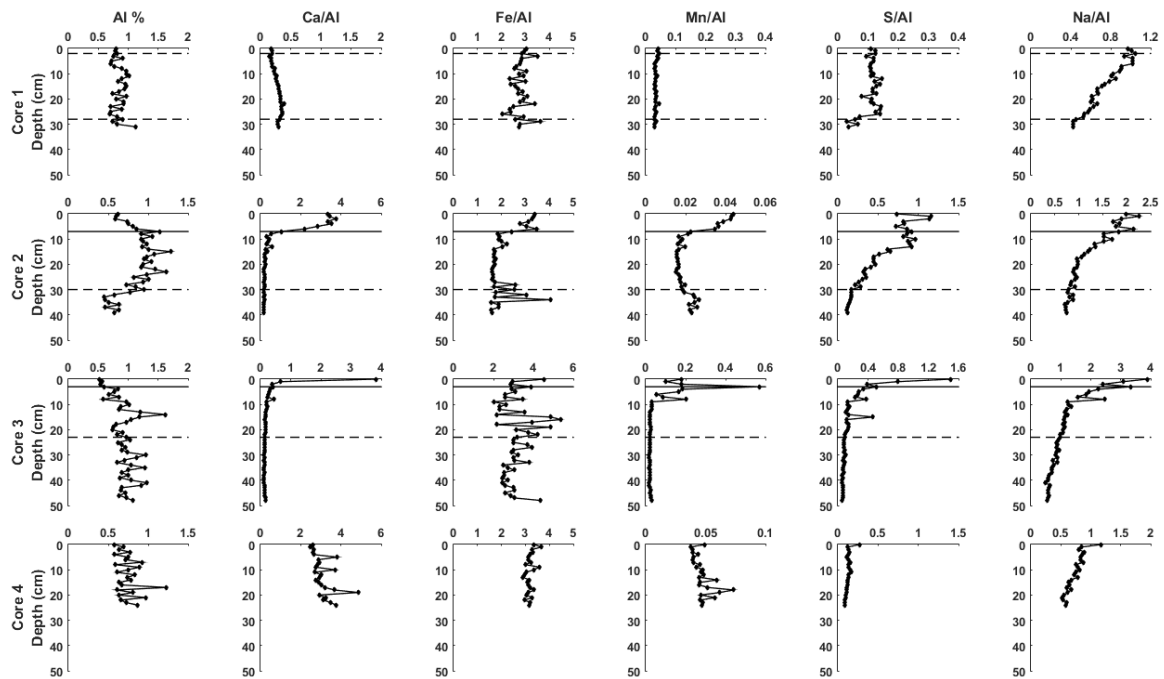**Figure 2:** Variations in Al, Ca, Fe, Mn, S and Na concentration with depth from the 2015 core samples.

Figure 3: Variations in Al, Ca, Fe, Mn, S and Na concentration with depth from the 2016 core samples.
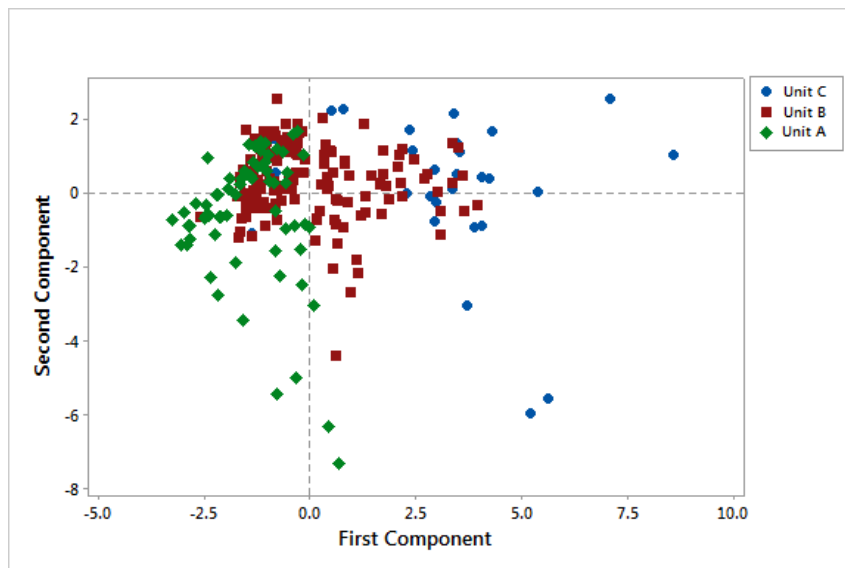

Figure 4: Principle component analysis (PCA) scores for the three sediment units identified in Cores 1 – 4 in 2015 and Cores 1 – 3 in 2016. Components 1 and 2 collectively accounted for 49.6 % of the total variance.
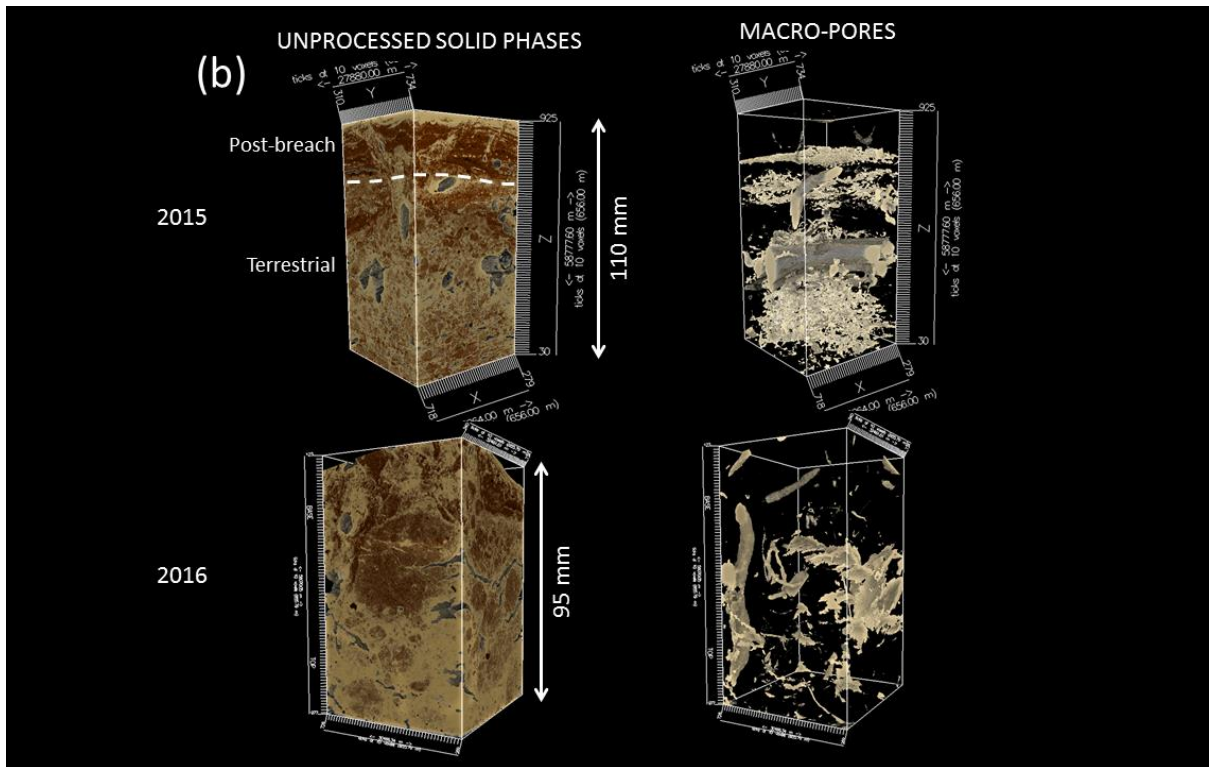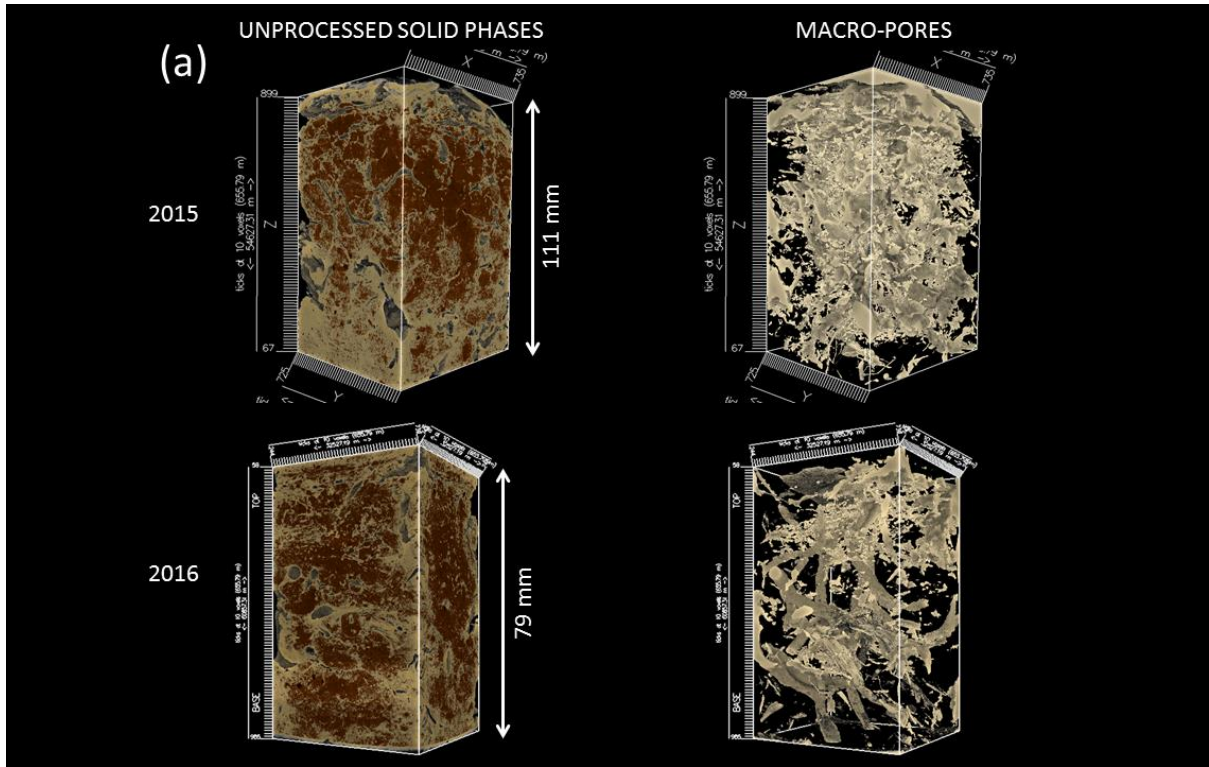
Figure 5: Reconstructions of sediment phases imaged used μCT analysis in (a) Core 1 and (b)
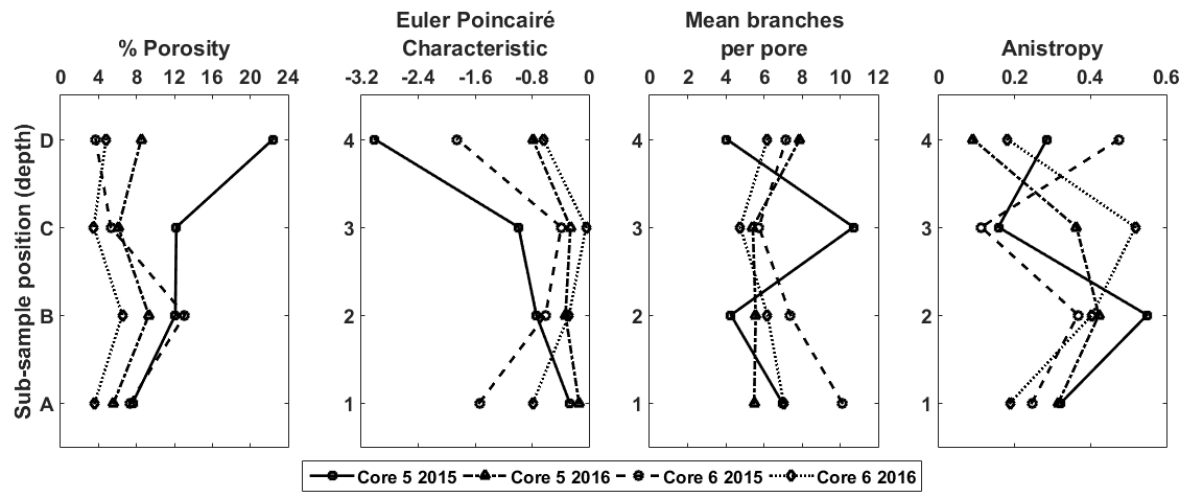
Core 2.

Figure 6: Porosity characteristics for sub-samples of Cores 5 and 6 in 2016 and 2017.
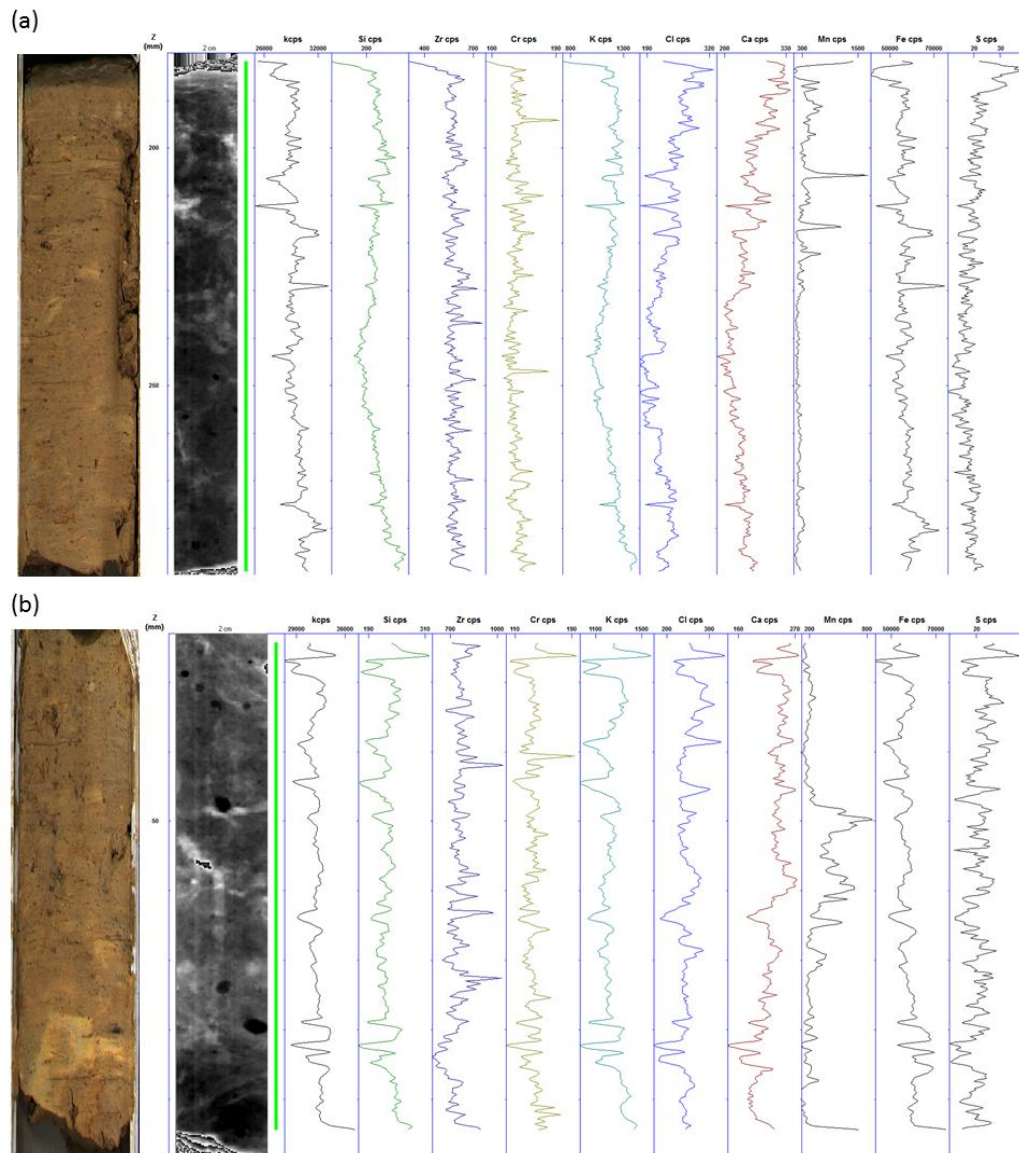
Figure 7: Si, Zr, Cr, K, Cl, Ca, Mn, Fe and S distribution, X-radiograph and photograph of core from (a) Core 5_{15}, (b) Core 5_{16}, (c) Core 6_{15} and (d) Core 6_{16}. Data are from Itrax scanning: X-axis shows X-ray response, y-axis represents depth.
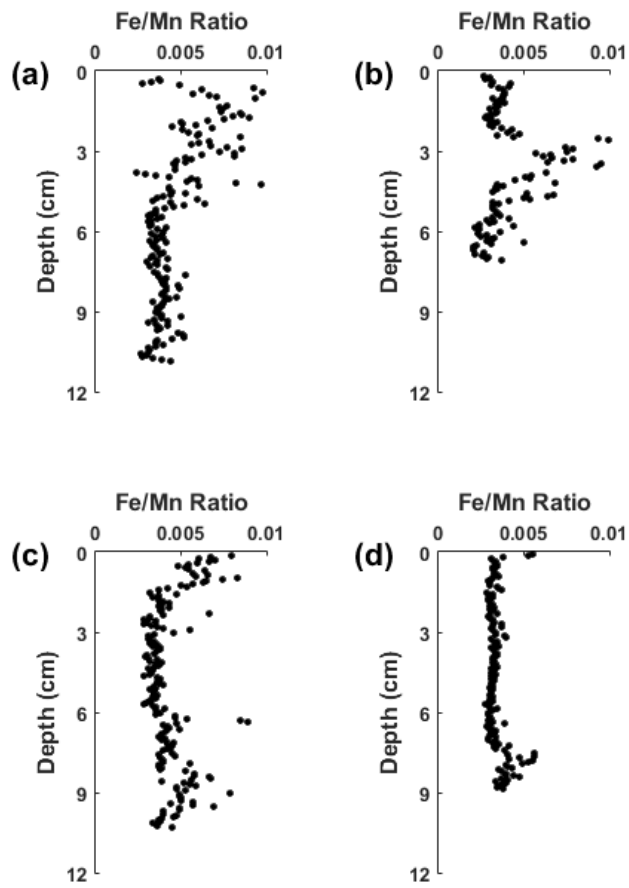
Figure 8: Fe / Mn ratio for (a) Core 5_{15}, (b) Core 5_{16}, (c) Core 6_{15} and (d) Core 6_{16} derived from Itrax geochemical data.

Tables

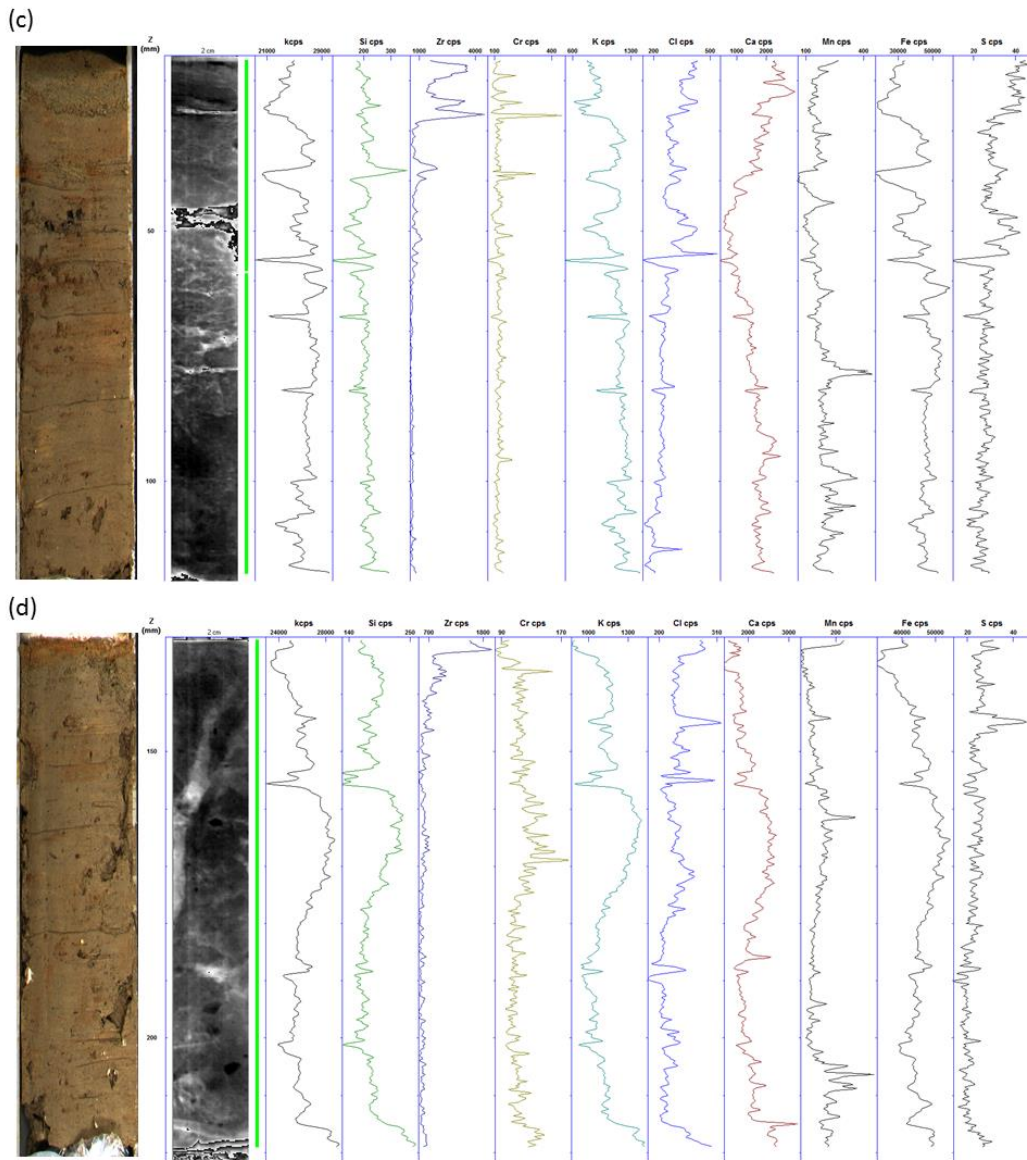**Table 1:** Former (terrestrial) land use at sampling locations within the Medmerry Managed Realignment Site and the proposed structural state.

Site	Terrestrial Land Use	Proposed Structure and Composition
Core 1	Low quality arable / pastoral land	Some compaction but interconnected pore networks still expected to be present
Core 2	Non-vegetated pastoral land	
Core 3	Vegetated pastoral land	Uncompact freely draining sediment
Core 4	Intensive arable field	Compact, with low abundance of pore networks resulting lower subsurface solute transfer and anoxic conditions

Table 2: Mean values for physical sediment characteristics for the three sediment units identified (see text for discussion) at the four coring sites (see Figure 1 for locations) in 2015 and 2016.

			Wet Bulk Density (kg m^{-3})		Moisture Content (%)		Porosity		Loss on Ignition (%)		Median Grain Size (µm)		Mud (clay + silt) Content (%)	
			Mean	SD	Mean	SD	Mean	SD	Mean	SD	Mean	SD	Mean	SD
Core 1	2015	Unit C	0.76	0.2	62.22	22.14	0.68	0.11	7.58	0.59	6.58	0.58	97.41	0.68
		Unit B	0.86	0.16	49.04	3.59	0.62	0.07	6.95	2.9	8.44	1.58	94.12	2.52
		Unit A	0.89	0.16	43.99	9.05	0.58	0.09	7.51	2.16	15.34	3.76	92.23	2.95
	2016	Unit C	1.94	0.34	44.82	0.78	0.5	0.09	6.79	11.33	6.03	1.88	89.83	9.77
		Unit B	1.88	0.22	46.42	3.49	0.52	0.06	6.16	5.49	6.71	1.05	87.28	5.25
		Unit A	2.08	0.35	41.84	4.86	0.44	0.11	4.07	3.74	6.19	0.41	91.2	1.45
Core 2	2015	Unit C	0.92	0.23	123.08	14.49	0.72	0.07	5.73	1.83	7.47	0.4	97.67	2.26
		Unit B	1.02	0.38	96.23	21.28	0.65	0.13	9.92	5.87	15.68	8.61	81.44	11.15
		Unit A	1.51	0.45	48.8	6.2	0.33	0.19	7.01	4.72	16.91	5.65	79.48	7.83
	2016	Unit C	1.48	0.27	100.92	5.59	0.72	0.05	4.96	6.15	10.05	2.04	77.36	6.76
		Unit B	1.39	0.33	97.37	29.84	0.73	0.09	12.48	8.54	11.51	7.96	68.23	9.39
		Unit A	1.75	0.3	40.69	8.3	0.53	0.1	4.83	11.1	33.15	25.68	54.1	14.62
Core 3	2015	Unit C	0.64	0.06	122.21	9.46	0.81	0.02	18.61	0.47	6.42	0.78	96.19	3.32
		Unit B	0.99	0.28	69.34	11.05	0.61	0.12	13.48	2.77	6.7	0.77	95.18	2.62
		Unit A	0.93	0.2	51.46	12.19	0.58	0.1	4.52	3.74	5.46	0.59	96.79	5.63
	2016	Unit C	1.39	0.21	118.04	26.02	0.76	0.03	19.21	3.65	11.06	0.86	73.86	3.16
		Unit B	1.71	0.28	69.06	17.39	0.61	0.09	9.88	6.89	7.46	2.46	84.49	7.96
		Unit A	2.18	0.28	40.66	3.64	0.41	0.08	3.24	8.7	7.39	3.25	84.81	9.4
Core 4	2015	Unit C	0.94	0.14	47.95	0.67	0.58	0.07	5.5	15.66	46.48	28.77	59.17	20.19
		Unit B	0.98	0.2	42.25	3.7	0.54	0.1	5.18	3.83	8.54	1.48	89.73	5.13
		Unit A	0.93	0.14	36.89	1.97	0.55	0.07	4.38	1.44	7.52	0.6	92.29	2.33
	2016		1.94	0.33	36.62	4.4	0.46	0.09	4.85	8.59	10.2	8.43	78.06	9.93

Table 3: Porosity analysis derived from µCT analysis divided into sub-samples. Data are presented based on different sediment facies. Core 5 was taken from an area of former lower intensity arable agriculture; Core 6 was taken from an area of former high intensity arable agriculture.

	% Macroporosity	Macro-pore abundance	Pore Connectivity (Euler-Poincairé Characteristic)	Pore network complexity (no. of braches per pore)	Pore Anisotropy
Core 5 2015 A-D	7.6 – 22.4	Low (mean 3672), particularly in the upper sub-sample	-3.01 – -0.27, increasing upwards apart from upper sub-sample	4.05 – 10.71 with no distinctive patterns evident	Moderately high (mean 0.33), although much higher in lower (A and B) sub-samples
Core 5 2016 A-D	5.6 – 6.1	High (mean 5265) although lower in the upper sub-sample	-0.79 – -0.14, increasing upwards apart from upper sub-sample	5.42 – 7.89. Higher in upper sub-sample compared to other three	Moderately high (mean 0.3), but particularly low in upper sub-sample
Core 6 2015 lower facies A-C	5.3 – 13.1	High (mean 5133) and decreasing with depth	-1.54 – 0.39, increasing upwards apart from upper sub-sample	5.74 – 10.11, decreasing upwards.	Moderately low (mean 0.24)
Core 6 2015 upper facies D (post-breach)	3.7	Very high (9458)	-1.85	7.17, greater than the preceding sub-sample	High (0.48)
Core 6 2016 A-D	3.5 – 6.5	Moderately high (mean 4608) and decreasing downwards	-0.79 – -0.04, increasing upwards apart from upper sub-sample	4.76 – 7.04, following same pattern as 2015 sample.	Moderately high (mean 0.32), although lower in upper and lower sub-samples (A and D)